Electronic Supporting Information

Meso-phenyltetrabenzotriazaporphyrin based double-decker lanthanide(III) complexes: synthesis, structure, spectral properties and electrochemistry

Victor E. Pushkarev,*[a,b] Valery V. Kalashnikov,[a] Alexander Yu. Tolbin,[a] Stanislav A. Trashin,[a] Nataliya E. Borisova,[b] Victor B. Rybakov,[b] Larisa G. Tomilova[a,b] and Nikolay S. Zefirov[a,b]

[a] *Institute of Physiologically Active Compounds, Russian Academy of Sciences, 1 Severny proezd, 142432 Chernogolovka, Moscow Region, RF. Fax: +7 496 524 9508; E-mail: pushkarev@org.chem.msu.ru*

[b] *Department of Chemistry, M.V. Lomonosov Moscow State University, 1 Leninskie Gory, 119991 Moscow, RF. Fax: +7 495 939 0290; E-mail: tom@org.chem.msu.ru*

Contents list

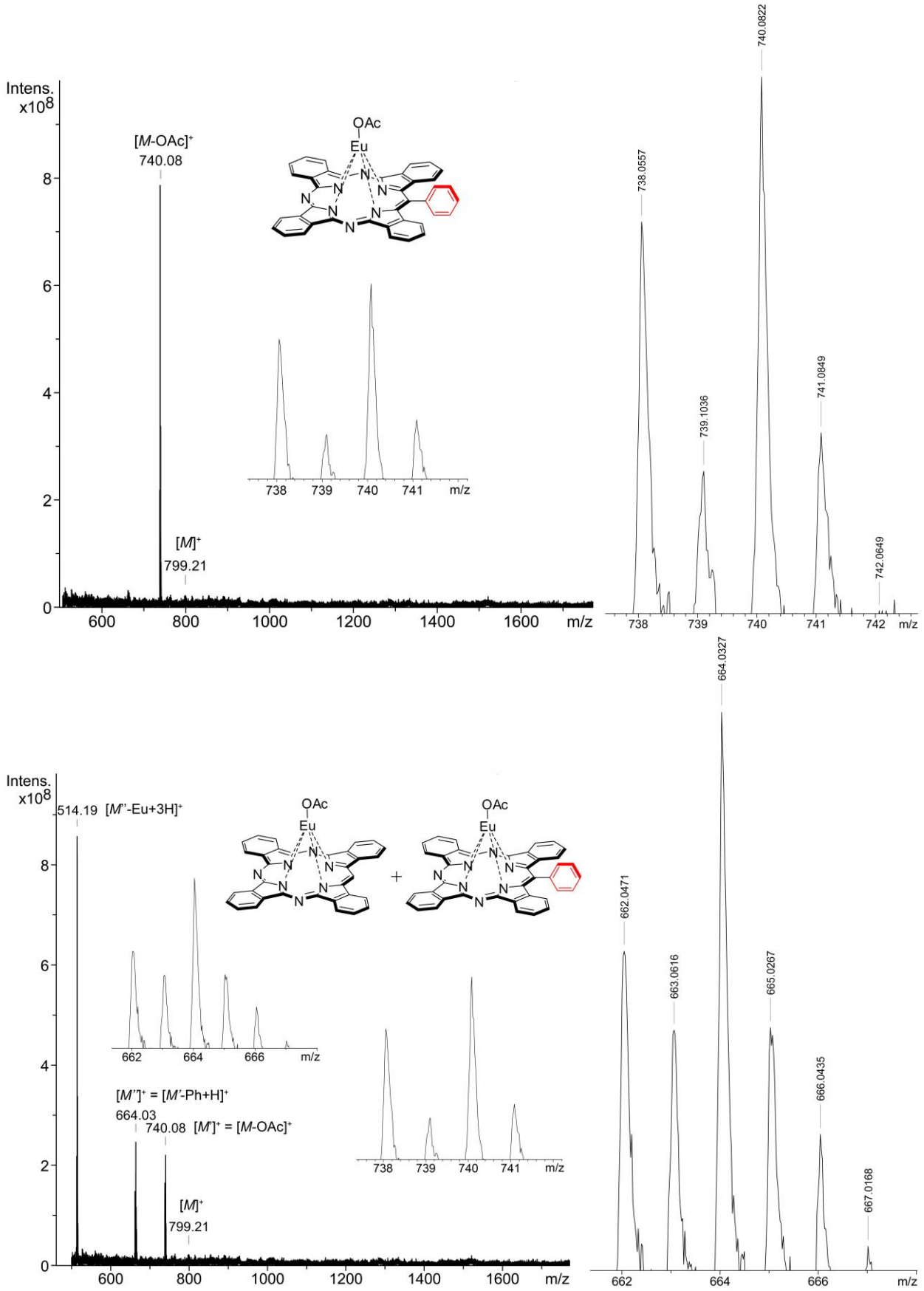

Fig. S1 MALDI-TOF mass spectra of the products of the synthesis of **2a**: top – reaction time 1h; bottom – reaction time 2h; isotopic patterns for the molecular ions are shown in insets. Isotopic distributions for the molecular ions of **2a** and its dearylation product by HR-MS mass spectrometry (right).

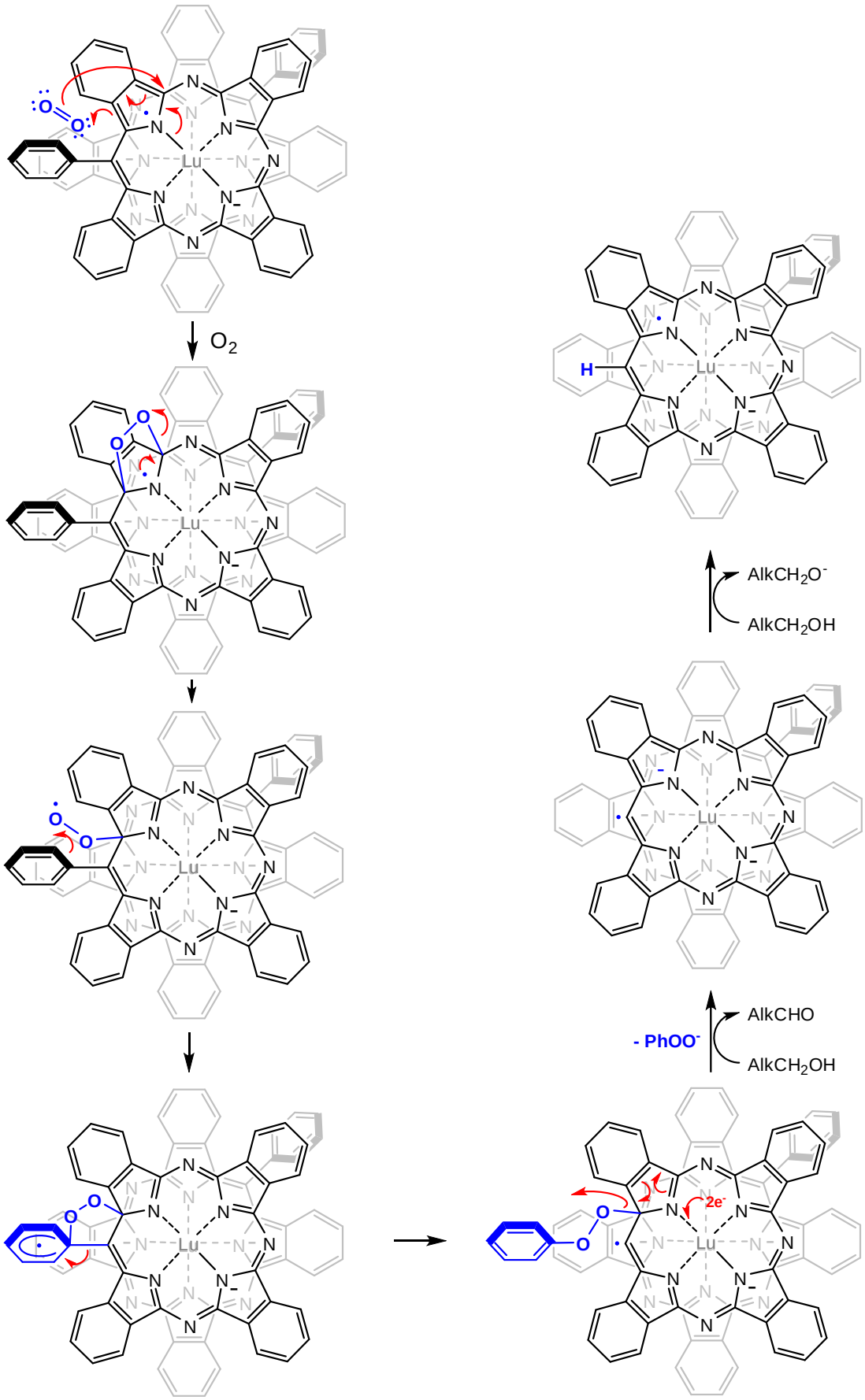

Fig. S2 Proposed dearylation mechanism on an example of complex **3b**.

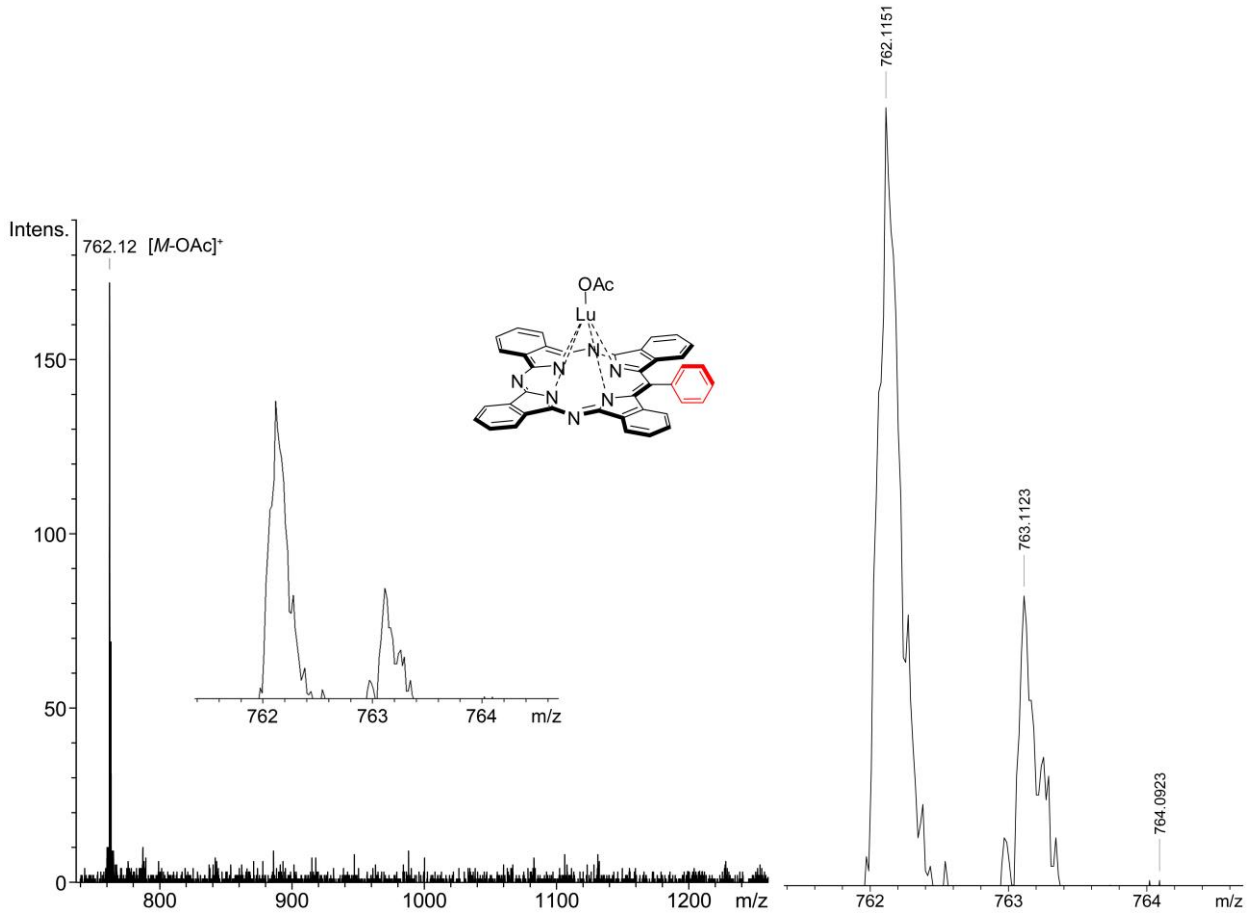

Fig. S3 MALDI-TOF mass spectrum of **2b** (left); isotopic pattern for the molecular ion is shown in inset. Isotopic distribution for the molecular ion of **2b** by HR-MS mass spectrometry (right).

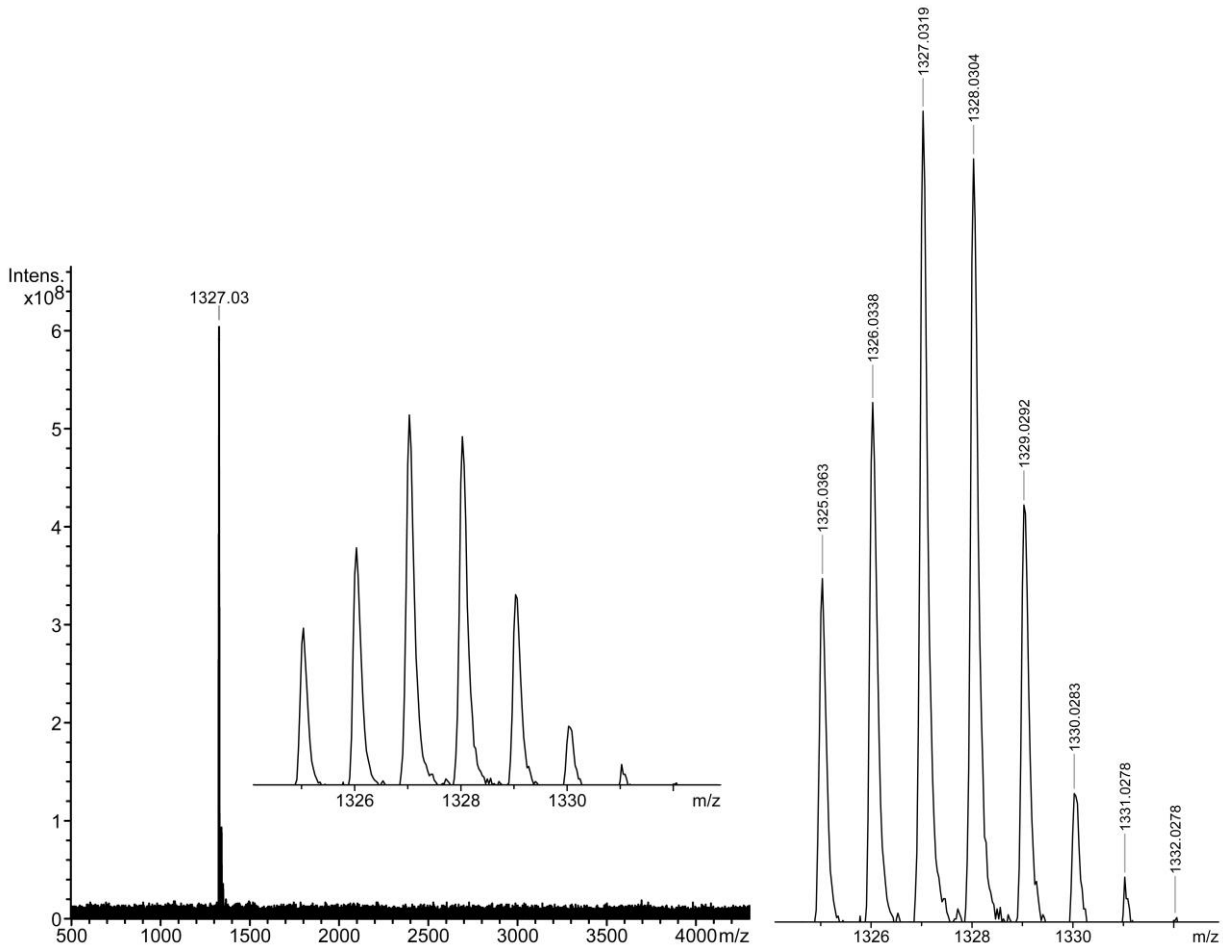

Fig. S4 MALDI-TOF mass spectrum of **3a** (left); isotopic pattern for the molecular ion is shown in inset. Isotopic distribution for the molecular ion of **3a** by HR-MS mass spectrometry (right).

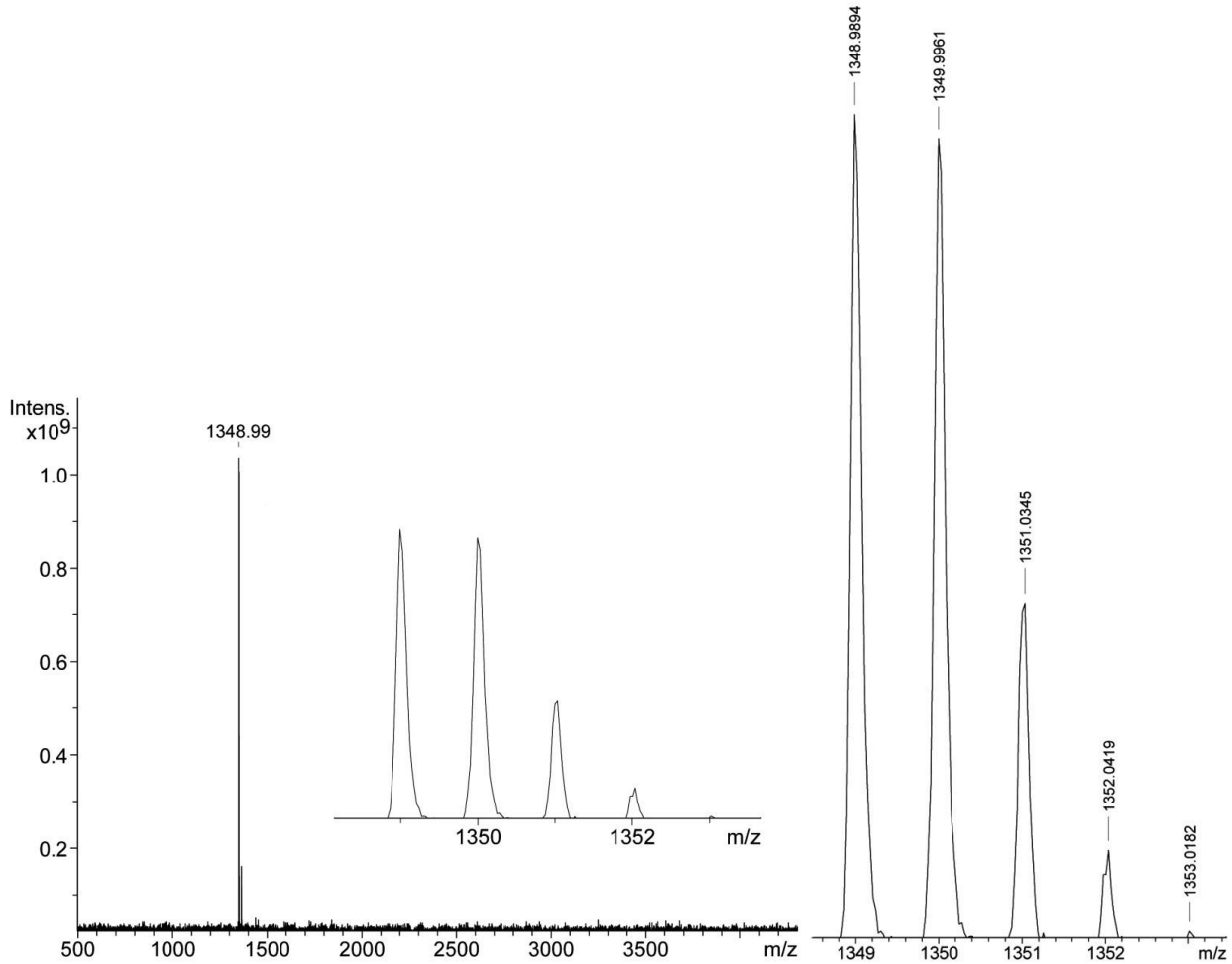

Fig. S5 MALDI-TOF mass spectrum of **3b** (left); isotopic pattern for the molecular ion is shown in inset. Isotopic distribution for the molecular ion of **3b** by HR-MS mass spectrometry (right).

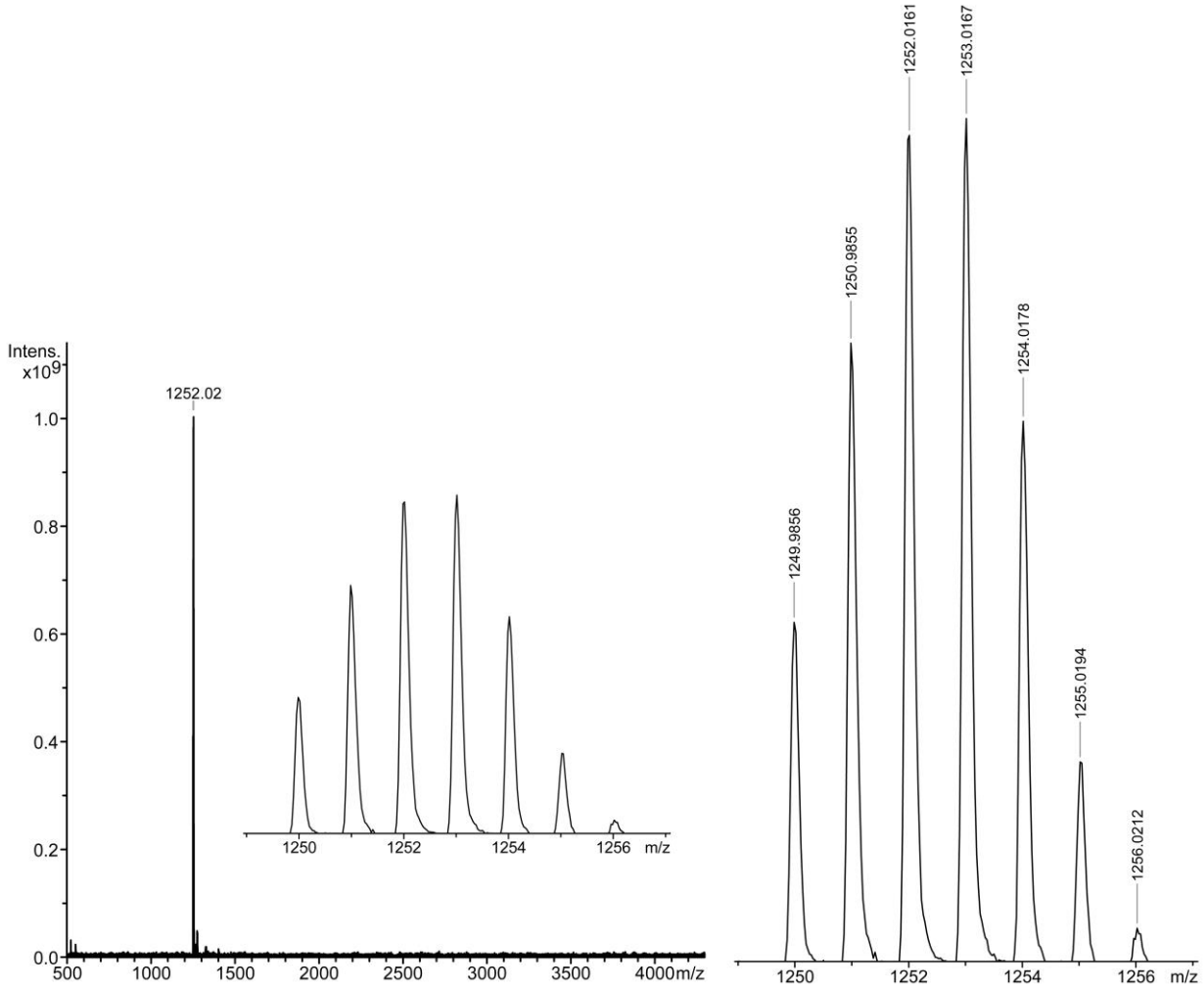

Fig. S6 MALDI-TOF mass spectrum of **4a** (left); isotopic pattern for the molecular ion is shown in inset. Isotopic distribution for the molecular ion of **4a** by HR-MS mass spectrometry (right).

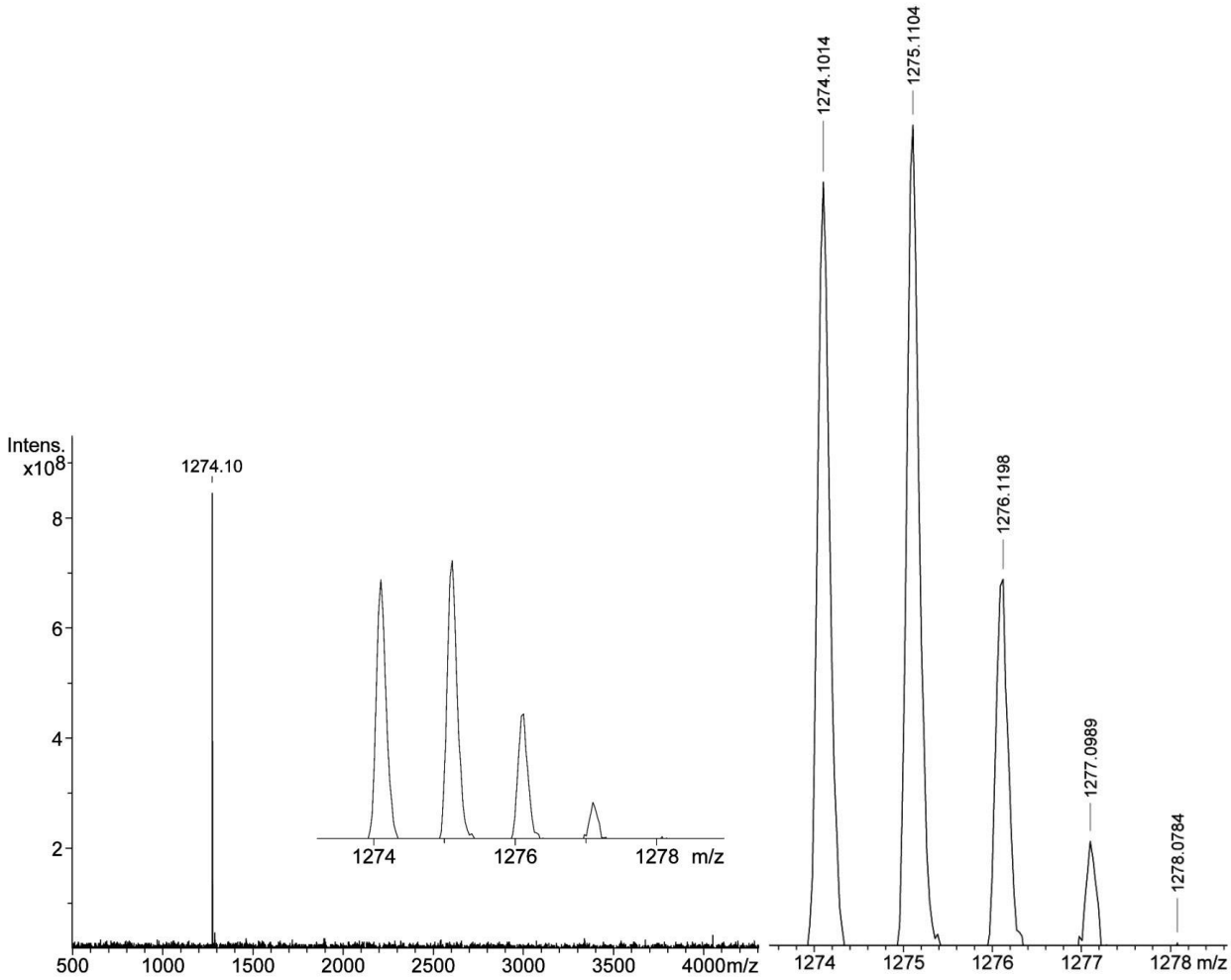

Fig. S7 MALDI-TOF mass spectrum of **4b** (left); isotopic pattern for the molecular ion is shown in inset. Isotopic distribution for the molecular ion of **4b** by HR-MS mass spectrometry (right).

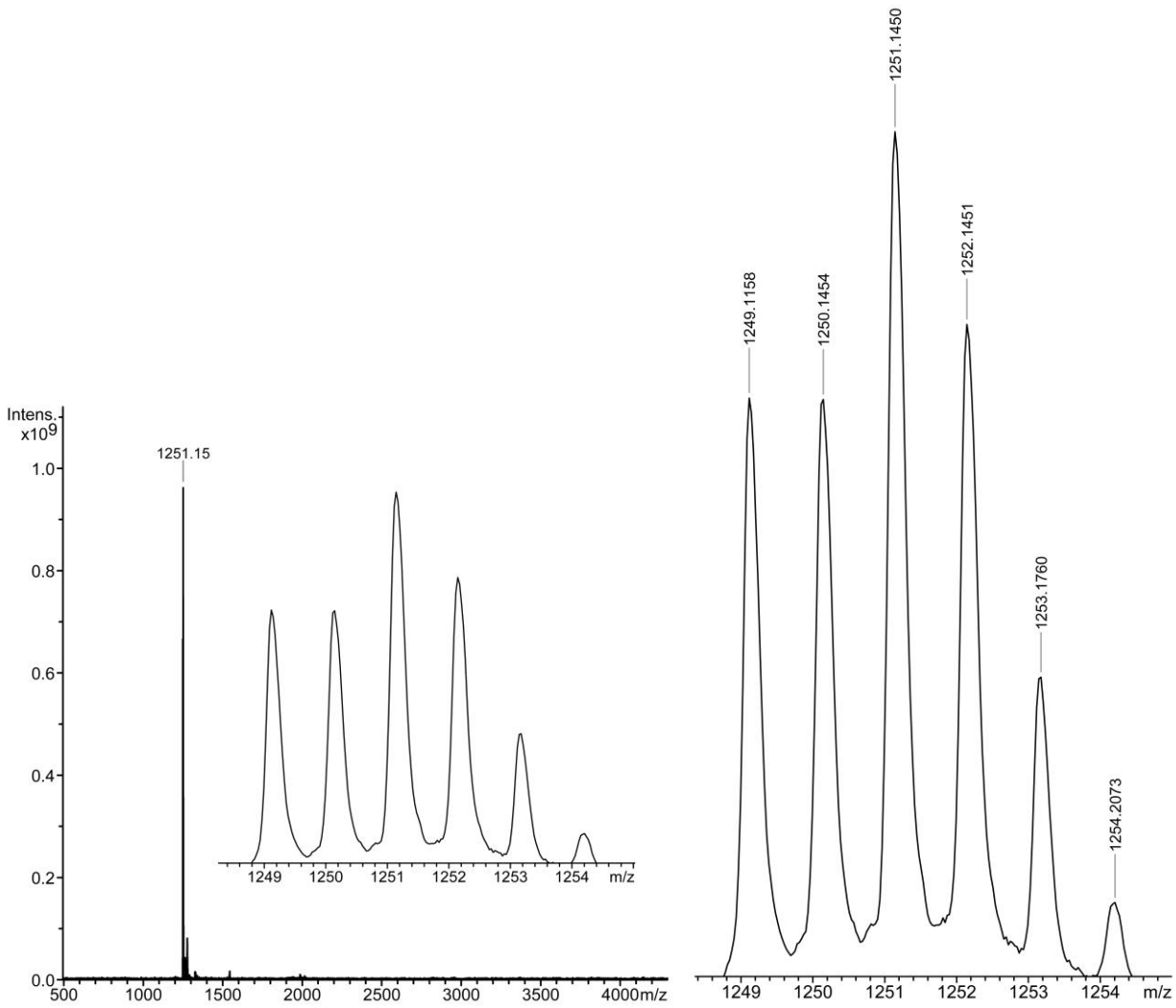

Fig. S8 MALDI-TOF mass spectrum of **5a** (left); isotopic pattern for the molecular ion is shown in inset. Isotopic distribution for the molecular ion of **5a** by HR-MS mass spectrometry (right).

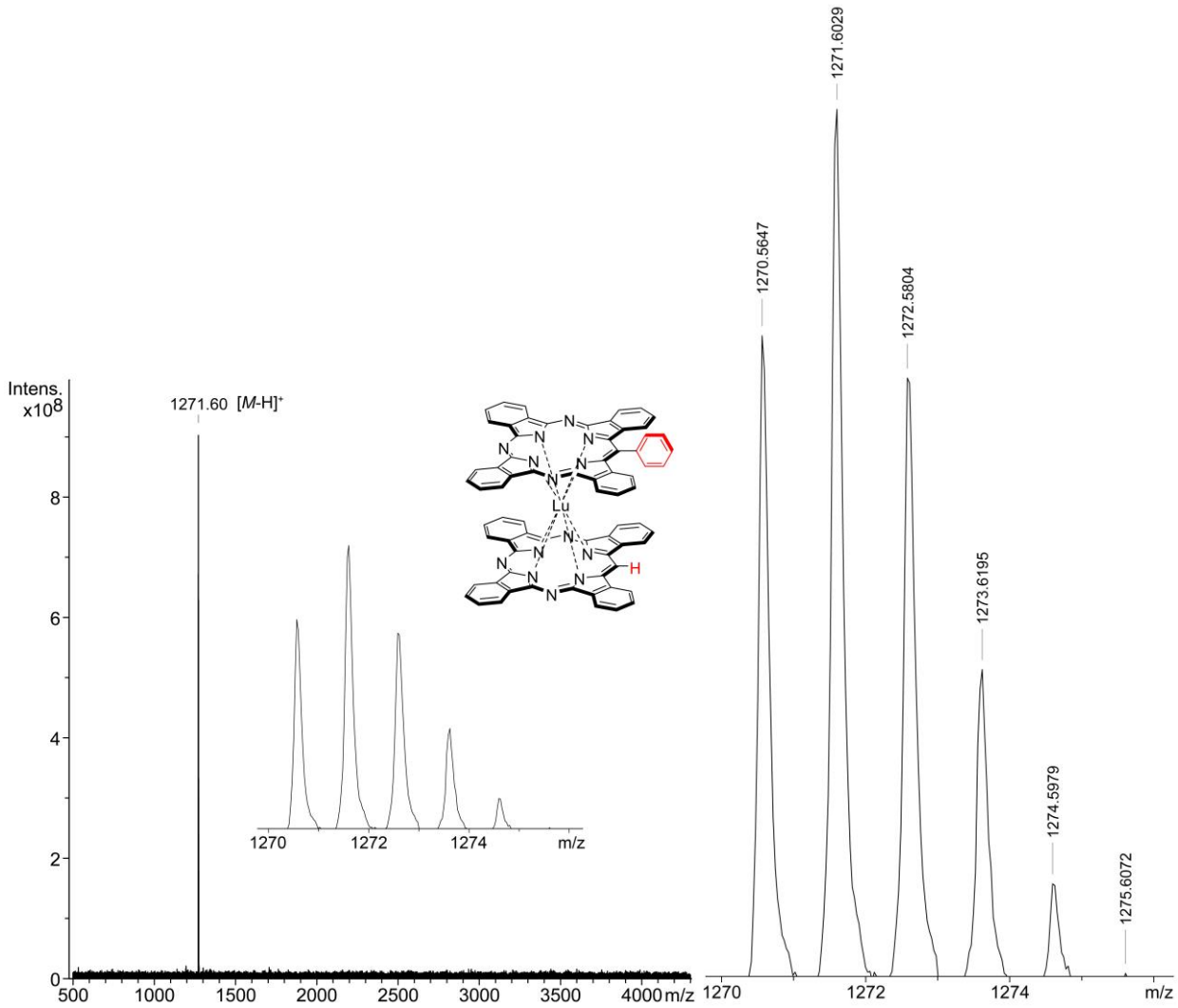

Fig. S9 MALDI-TOF mass spectrum of **5b** (left); isotopic pattern for the molecular ion is shown in inset. Isotopic distribution for the molecular ion of **5b** by HR-MS mass spectrometry (right).

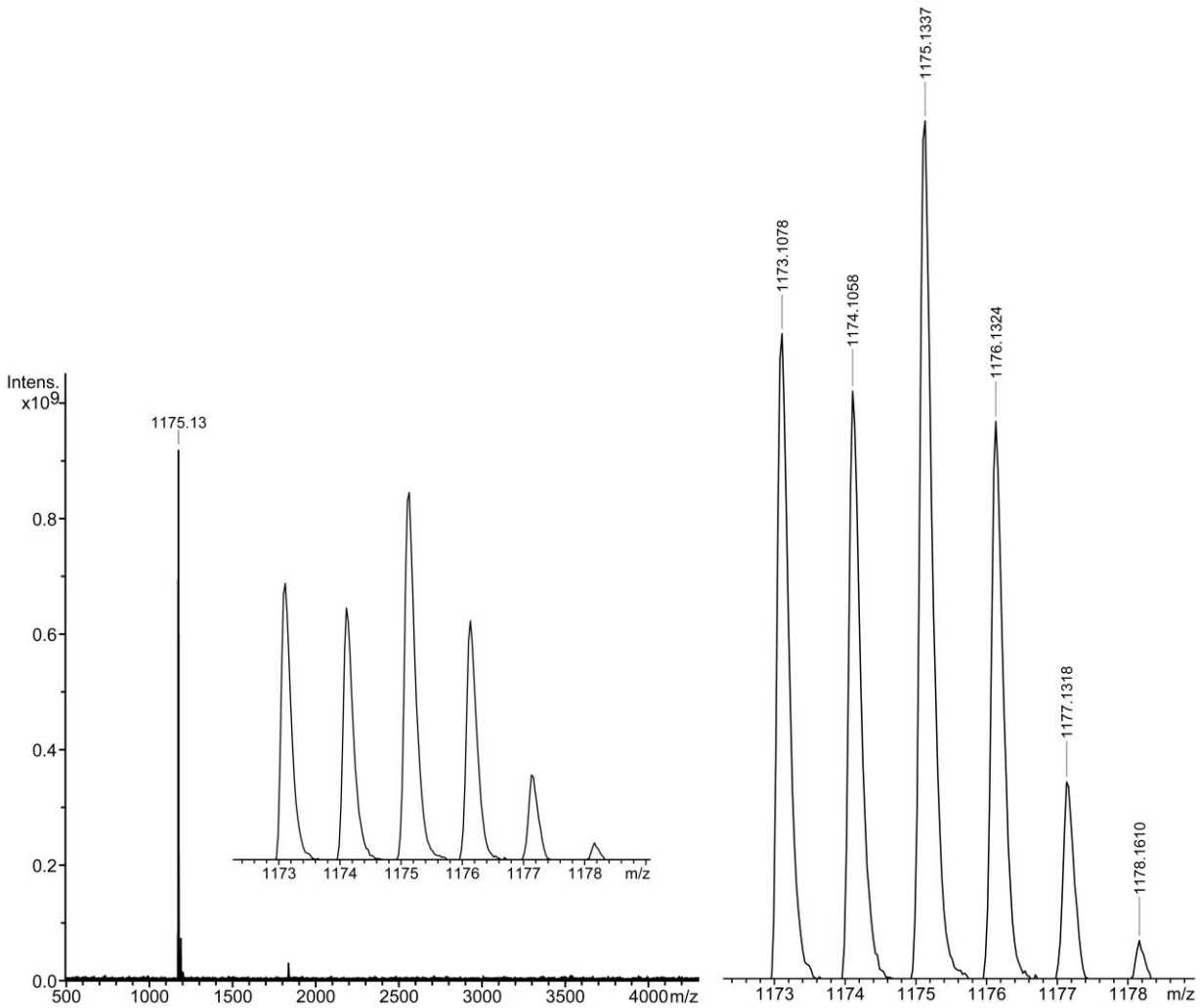

Fig. S10 MALDI-TOF mass spectrum of **6a** (left); isotopic pattern for the molecular ion is shown in inset. Isotopic distribution for the molecular ion of **6a** by HR-MS mass spectrometry (right).

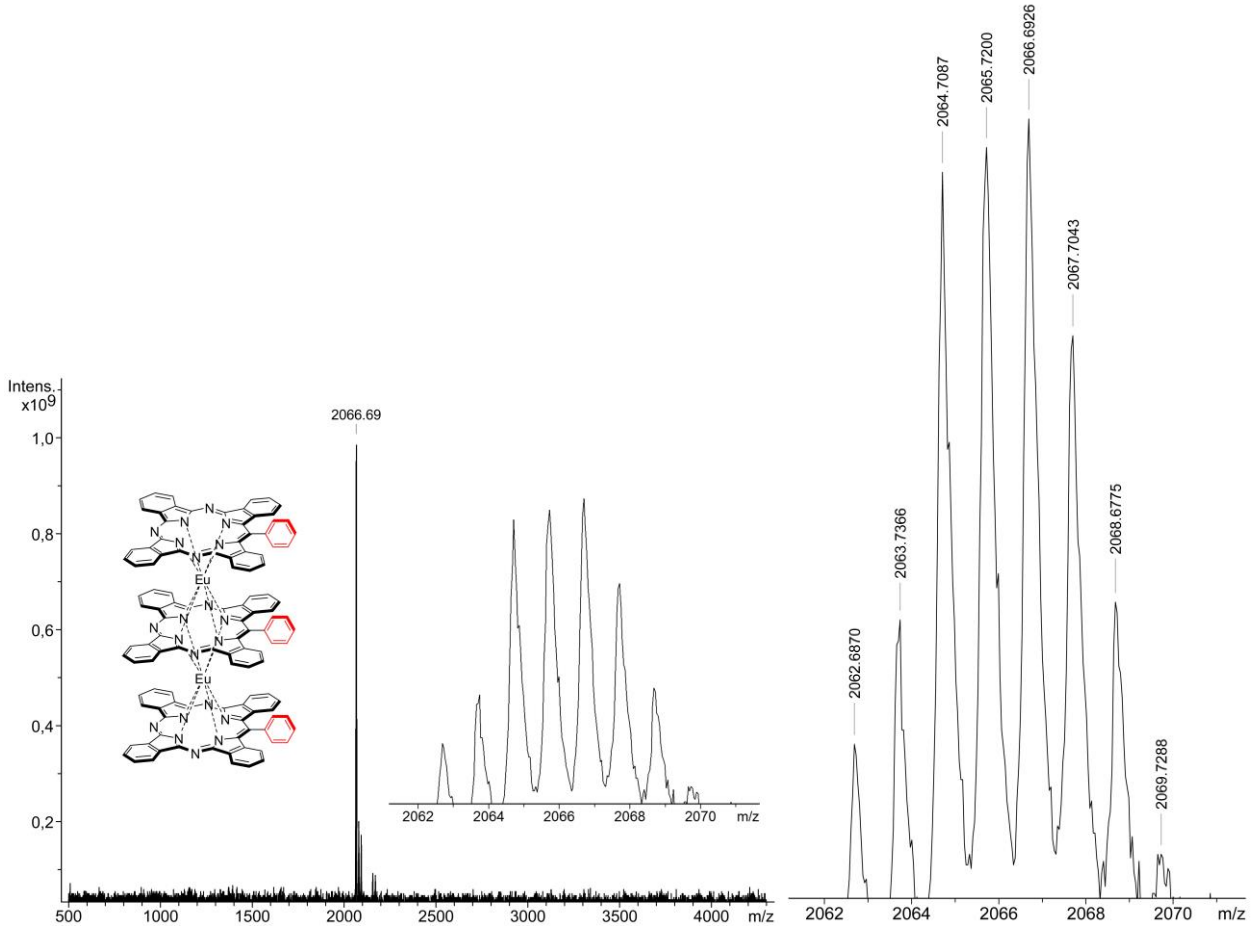

Fig. S11 MALDI-TOF mass spectrum of **7a** (left); isotopic pattern for the molecular ion is shown in inset. Isotopic distribution for the molecular ion of **7a** by HR-MS mass spectrometry (right).

(^{Ph}TBTAP)EuOAc (2a), $C_{39}H_{21}N_7Eu$, $[M–OAc]^+$ (theory 740.1071)

mass %
738 84.0 _____
739 37.8 _____
740 100.0 _____
741 42.4 _____
742 9.2 _____
743 1.3 _
744 0.1

(^{Ph}TBTAP)LuOAc (2b), $C_{39}H_{21}N_7Lu$, $[M–OAc]^+$ (theory 762.1266)

mass %
762 100.0 _____
763 47.6 _____
764 11.1 _____
765 1.7 _
766 0.2
767 0.0

(^{Ph}TBTAP)$_2$Eu (3a), $C_{78}H_{42}N_{14}Eu$, $[M]^+$ (theory 1327.2930)

mass %
1325 67.0 _____
1326 60.3 _____
1327 100.0 _____
1328 73.7 _____
1329 31.0 _____
1330 8.9 ____
1331 1.9 _
1332 0.3
1333 0.0

(^{Ph}TBTAP)$_2$Lu (3b), $C_{78}H_{42}N_{14}Lu$, $[M]^+$ (theory 1349.3125)

mass %
1349 100.0 _____
1350 92.7 _____
1351 42.4 _____
1352 12.8 _____
1353 2.8 _
1354 0.5
1355 0.1
1356 0.0

(^{Ph}TBTAP)EuPc (4a), $C_{71}H_{37}N_{15}Eu$, $[M]^+$ (theory 1252.2569)

mass %
1250 70.0 _____
1251 57.9 _____
1252 100.0 _____
1253 69.5 _____
1254 27.1 _____
1255 7.2 ____
1256 1.4 _
1257 0.2

(^{Ph}TBTAP)LuPc (4b), $C_{71}H_{37}N_{15}Lu$, $[M]^+$ (theory 1274.2764)

mass %
1274 100.0 _____
1275 85.4 _____
1276 36.0 _____
1277 10.0 _____
1278 2.0 _
1279 0.4
1280 0.0

(^{Ph}TBTAP)Eu(^{H}TBTAP) (5a), $C_{72}H_{38}N_{14}Eu$, $[M]^+$ (theory 1251.2616)

mass %
1249 69.7 _____
1250 58.1 _____
1251 100.0 _____
1252 70.0 _____
1253 27.4 _____
1254 7.3 ____
1255 1.4 _
1256 0.2

(^{Ph}TBTAP)Lu(^{H}TBTAP) (5b), $C_{72}H_{37}N_{14}Lu$, $[M–H]^+$ (theory 1272.2733)

mass %
1272 100.0 _____
1273 86.1 _____
1274 36.6 _____
1275 10.3 _____
1276 2.1 _
1277 0.4
1278 0.0

(^{H}TBTAP)$_2$Eu (6a), $C_{66}H_{34}N_{14}Eu$, $[M]^+$ (theory 1175.2303)

mass %
1173 72.3 _____
1174 55.6 _____
1175 100.0 _____
1176 65.9 _____
1177 24.0 _____
1178 5.9 ___
1179 1.0
1180 0.2

(^{Ph}TBTAP)$_3$Eu$_2$ (7a), $C_{117}H_{63}N_{21}Eu_2$, $[M]^+$ (theory 2066.3922)

mass %
2063 29.9 _____
2064 40.3 _____
2065 92.2 _____
2066 100.0 _____
2067 98.4 _____
2068 75.2 _____
2069 41.0 _____
2070 16.6 _____
2071 5.2 ___
2072 1.3 _
2073 0.3
2074 0.0

Fig. S12 Corresponding simulated MS patterns of the molecular ions for complexes **2**–**7**.

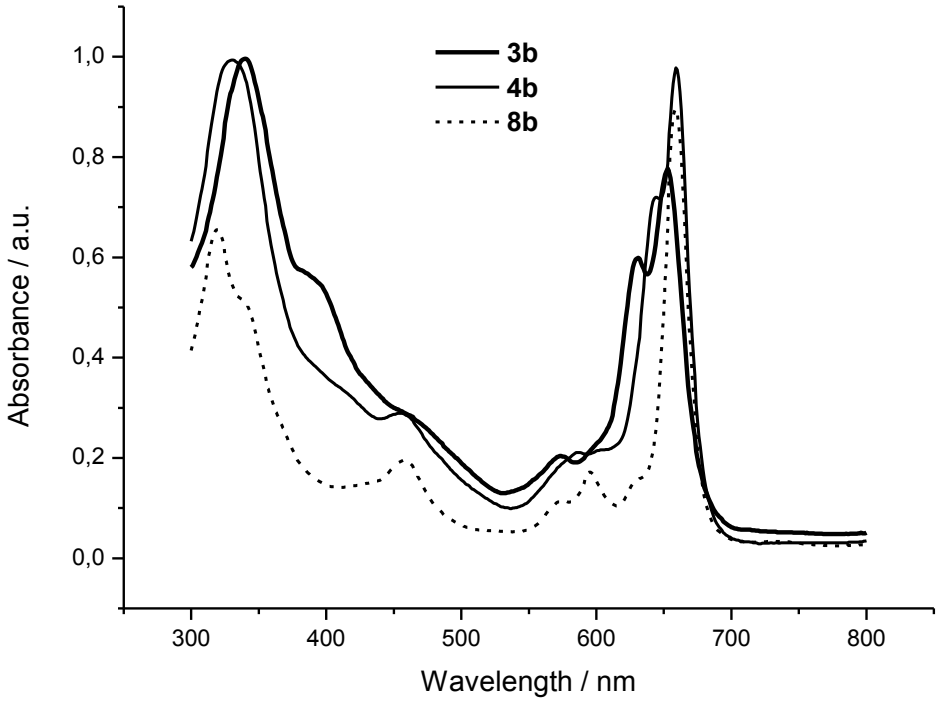

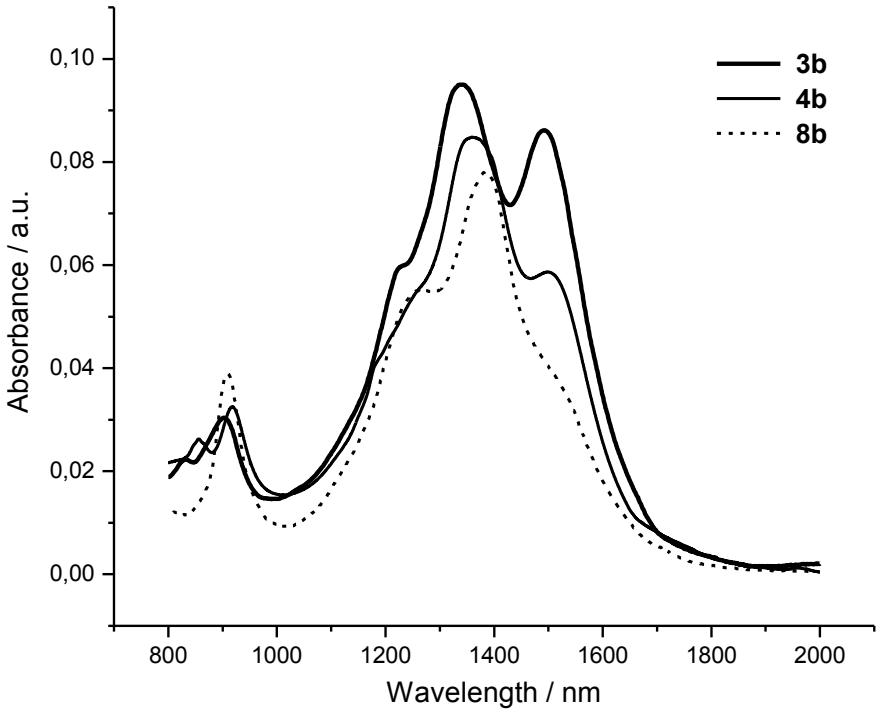

Fig. S13 UV-Vis and NIR spectra of **3b**, **4b** and **8b** in CCl_4.

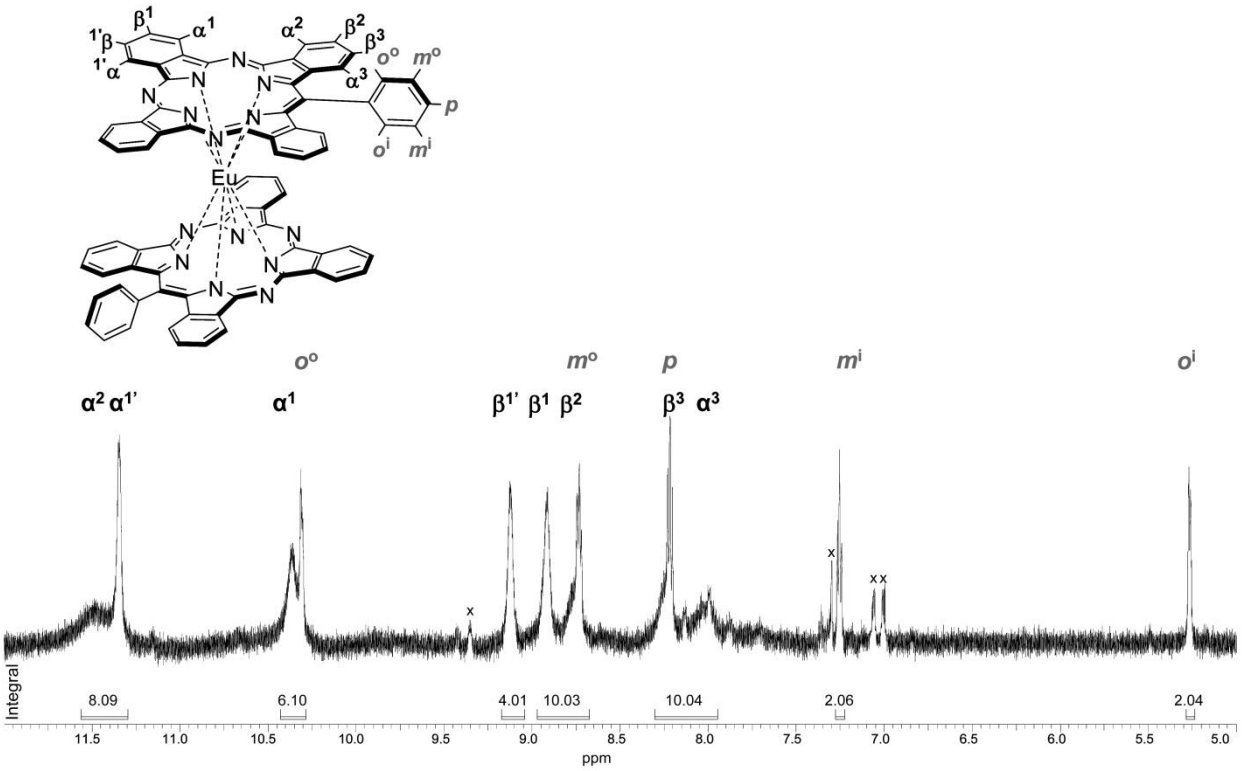

Fig. S14 ^{1}H NMR spectrum of **3a** (aromatic region) in [D_8]THF with the addition of sodium metal.

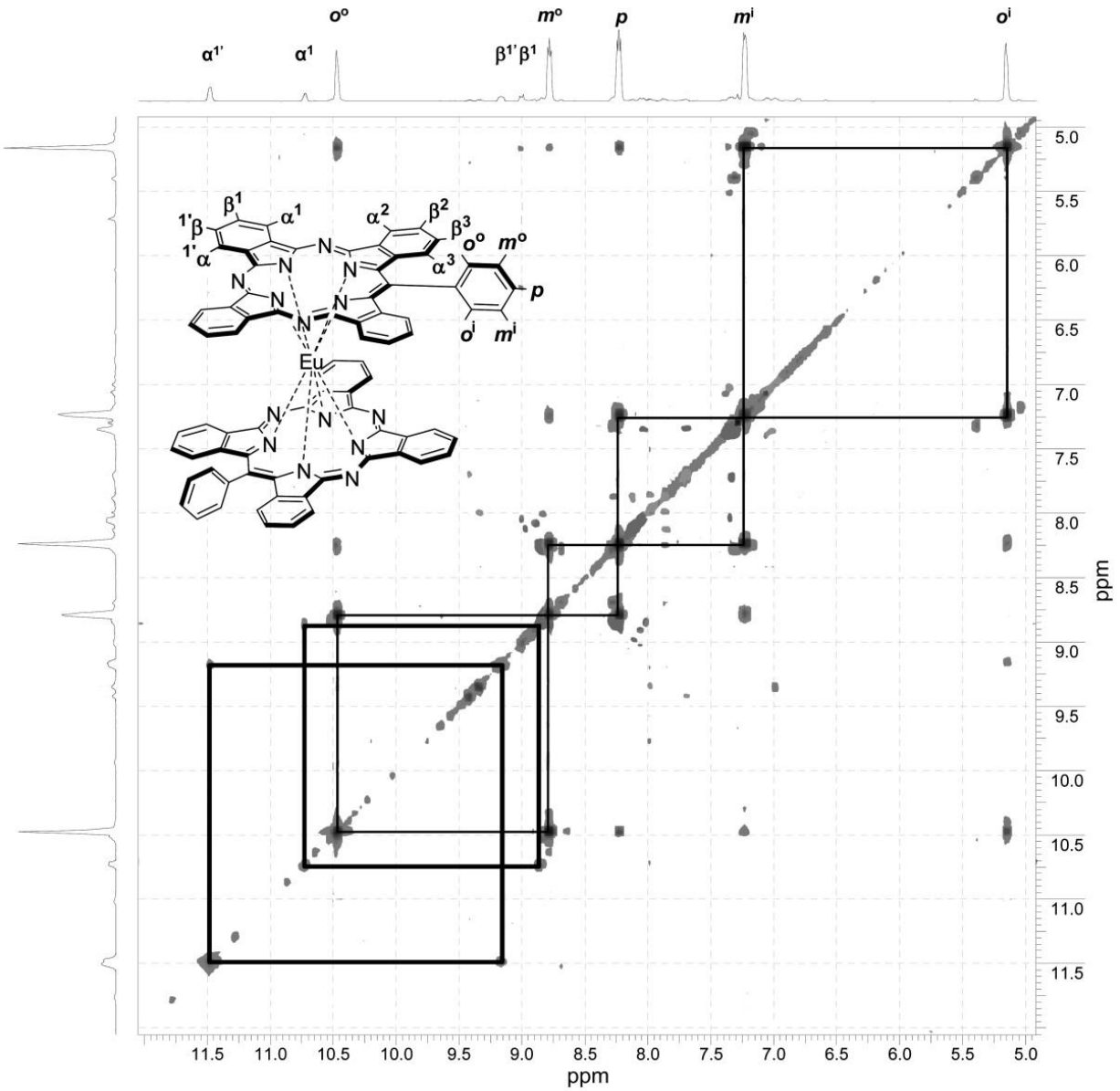

Fig. S15 $^{1}H–^{1}H$ COSY NMR spectrum of **3a** (aromatic region) in $[D_8]$THF with the addition of sodium metal.

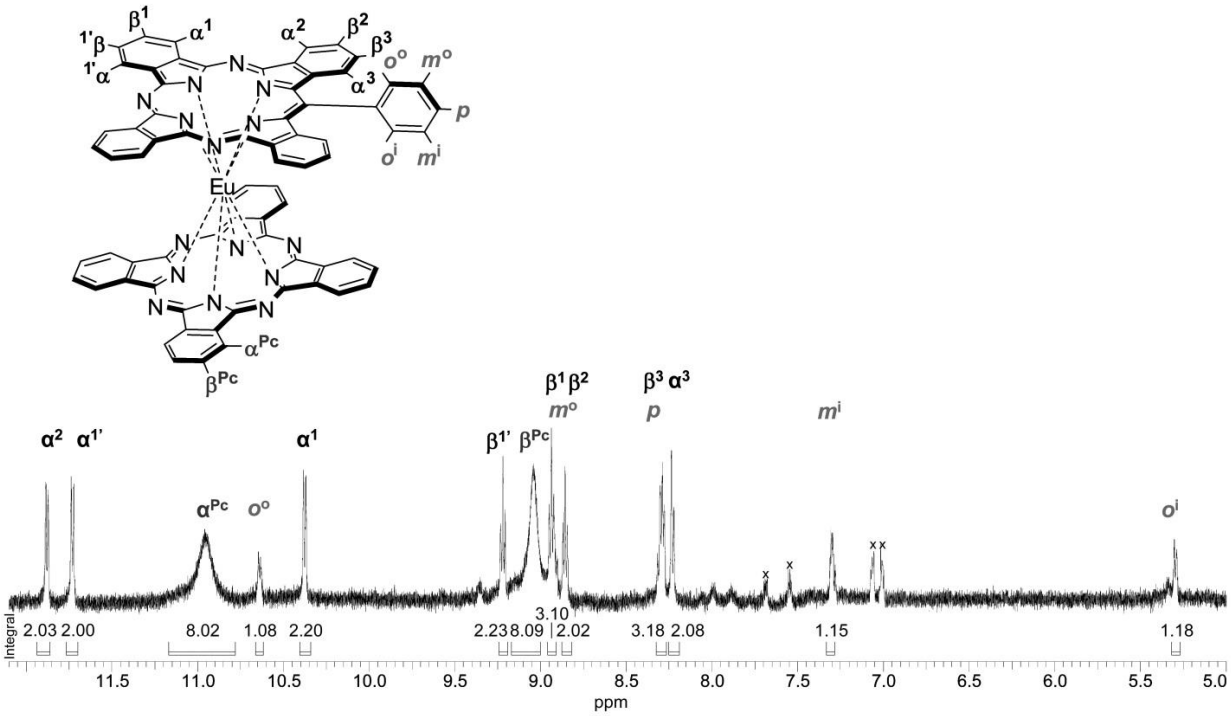

Fig. S16 ^{1}H NMR spectrum of **4a** (aromatic region) in [D_8]THF with the addition of sodium metal.

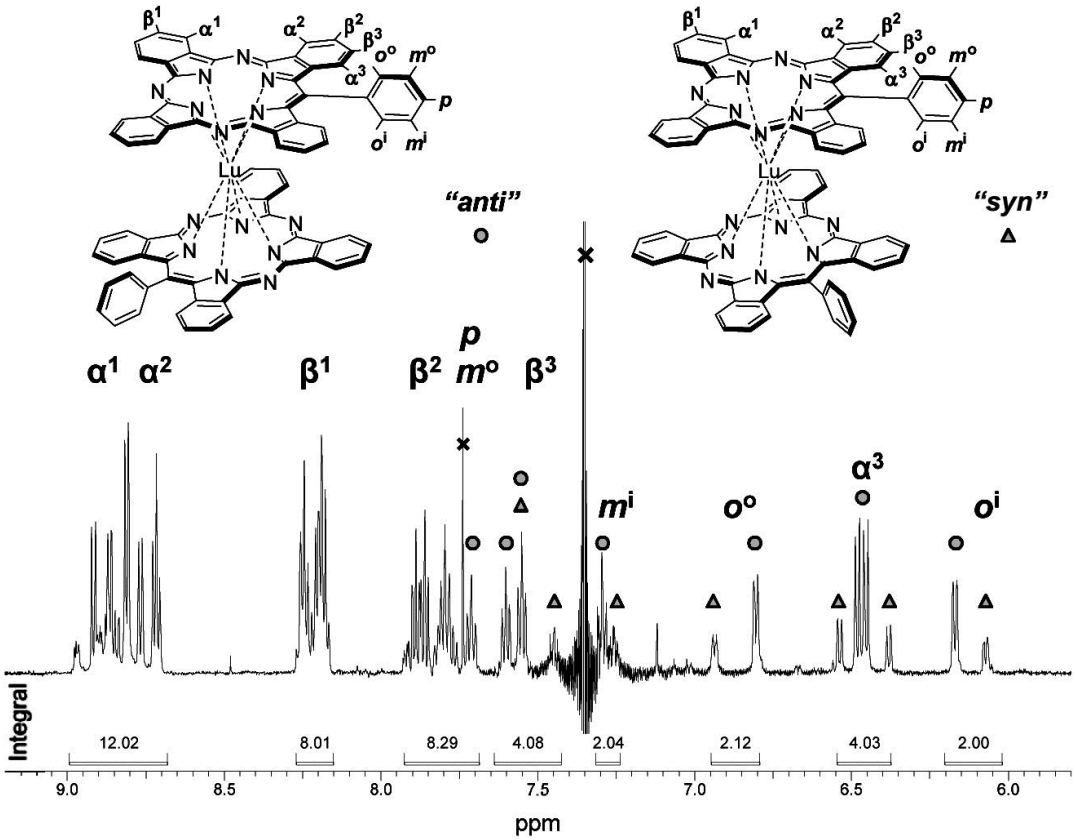

Fig. S17 ^{1}H NMR spectrum of **3b** (aromatic region) in [D_6]DMSO with the addition of 1–2 vol% $N_2H_4 \cdot H_2O$; distinct signals of the main "*anti*" and minor "*syn*" rotamer are marked with circles and triangles respectively; "×" indicates signals from residual solvents.

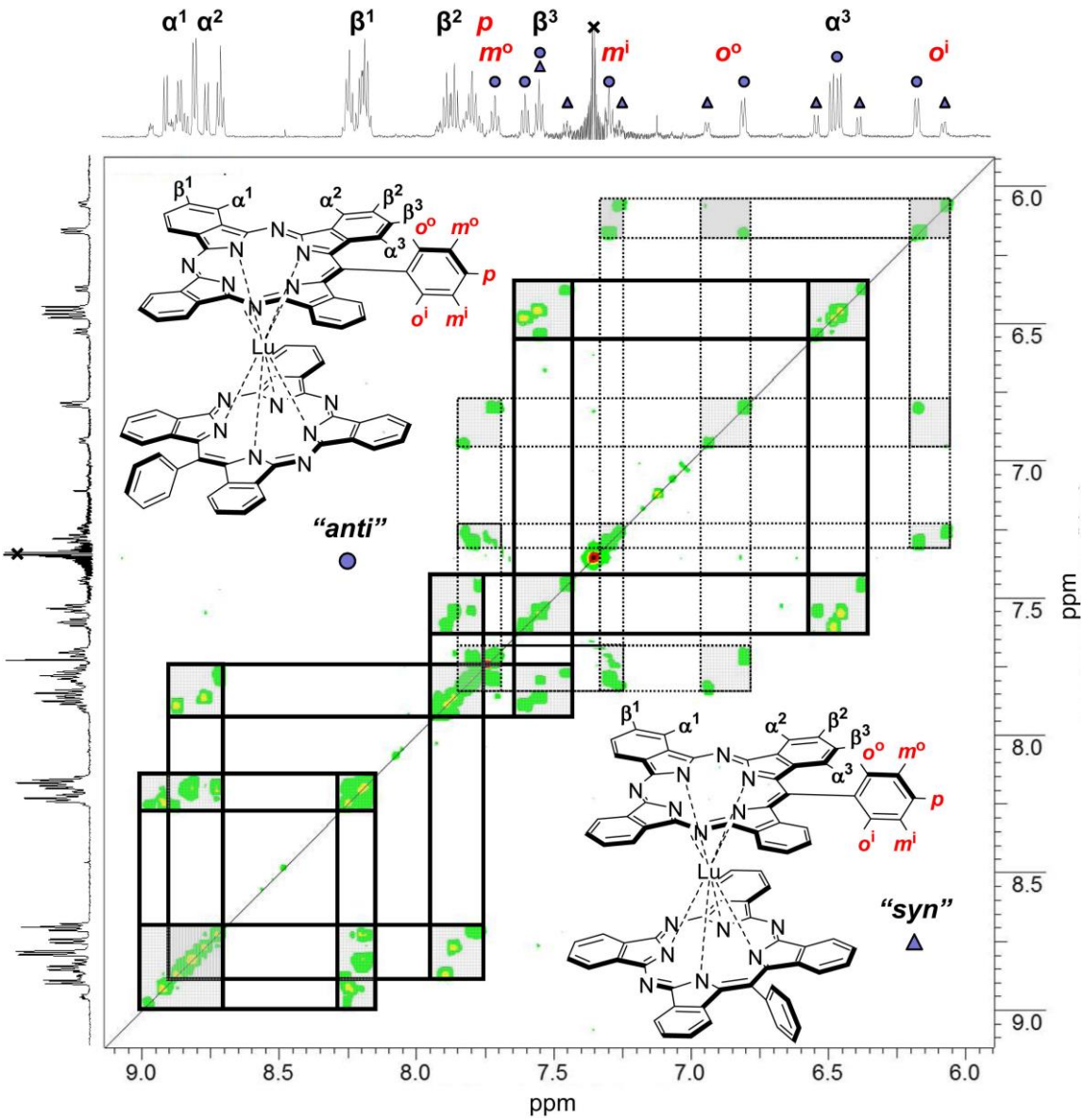

Fig. S18 ^{1}H–^{1}H COSY NMR spectrum of **3b** (aromatic region) in [D_6]DMSO with the addition of 1–2 vol% $N_2H_4 \cdot H_2O$.

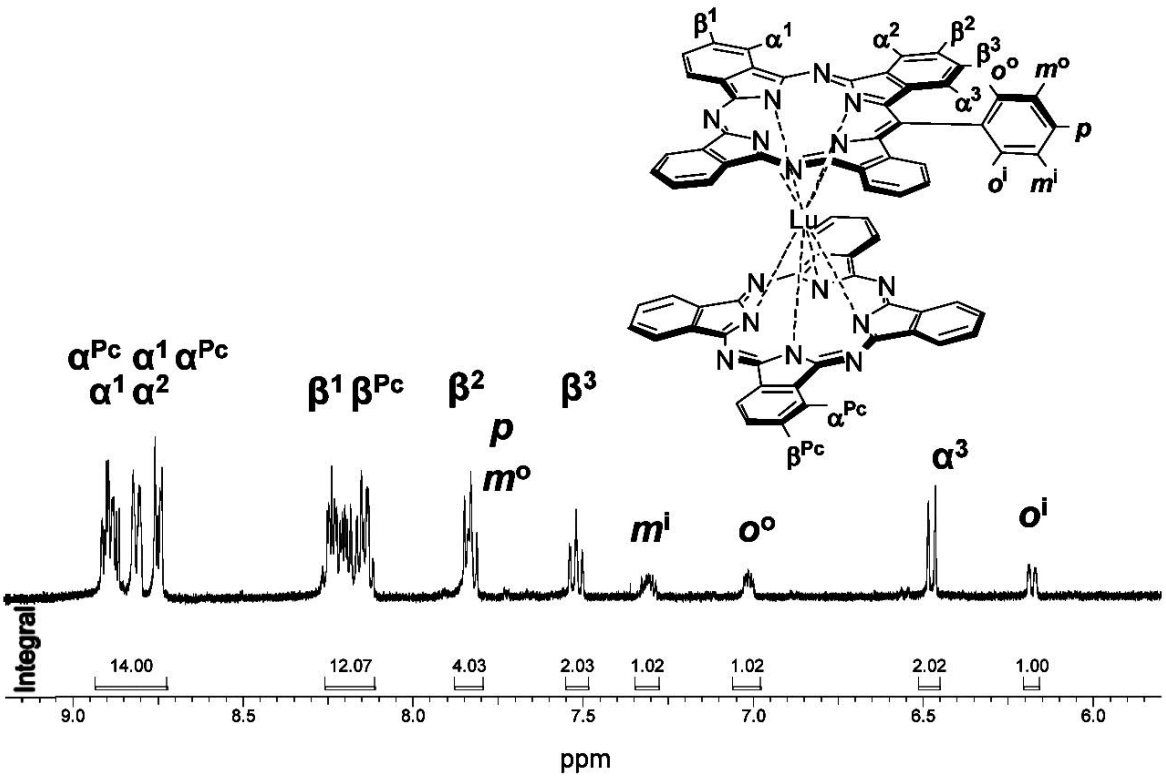

Fig. S19 ^{1}H NMR spectrum of compound **4b** (aromatic region) in [D_6]DMSO with the addition of 1–2 vol% $N_2H_4 \cdot H_2O$.

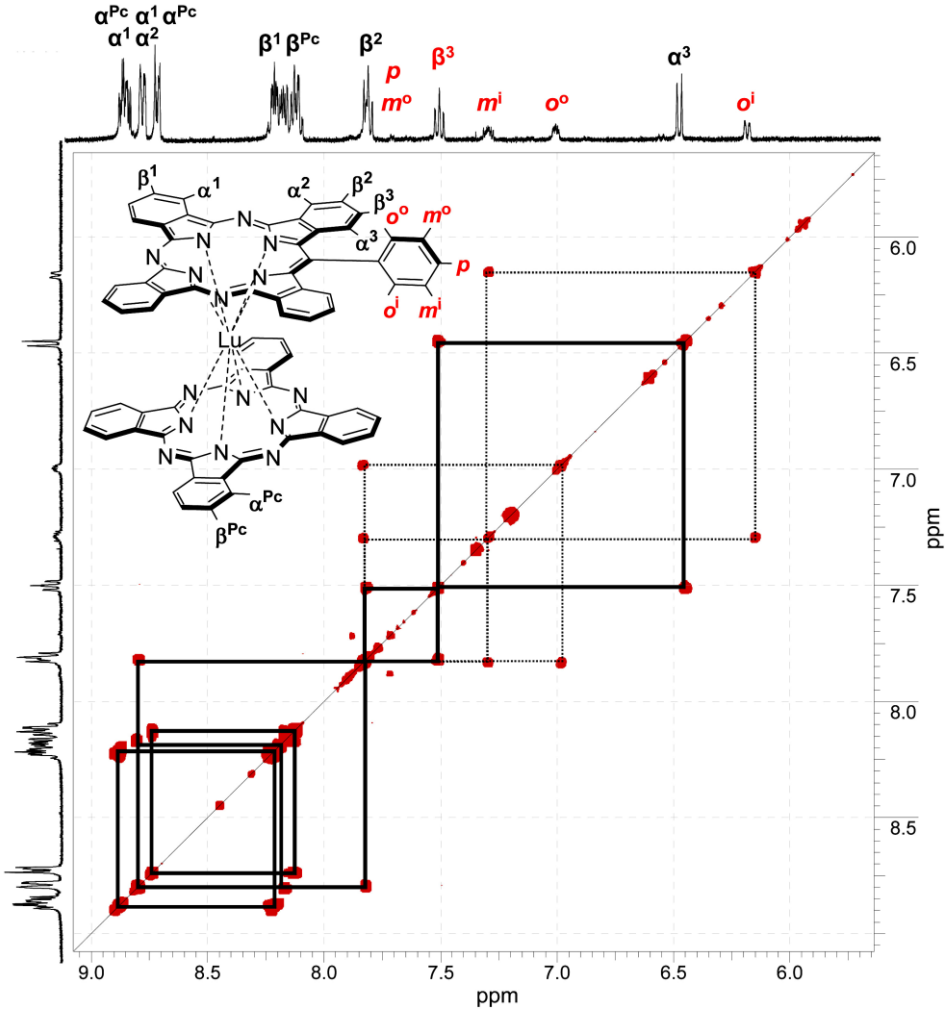

Fig. S20 ^{1}H–^{1}H COSY NMR spectrum of **4b** (aromatic region) in [D_6]DMSO with the addition of 1–2 vol% $N_2H_4 \cdot H_2O$.

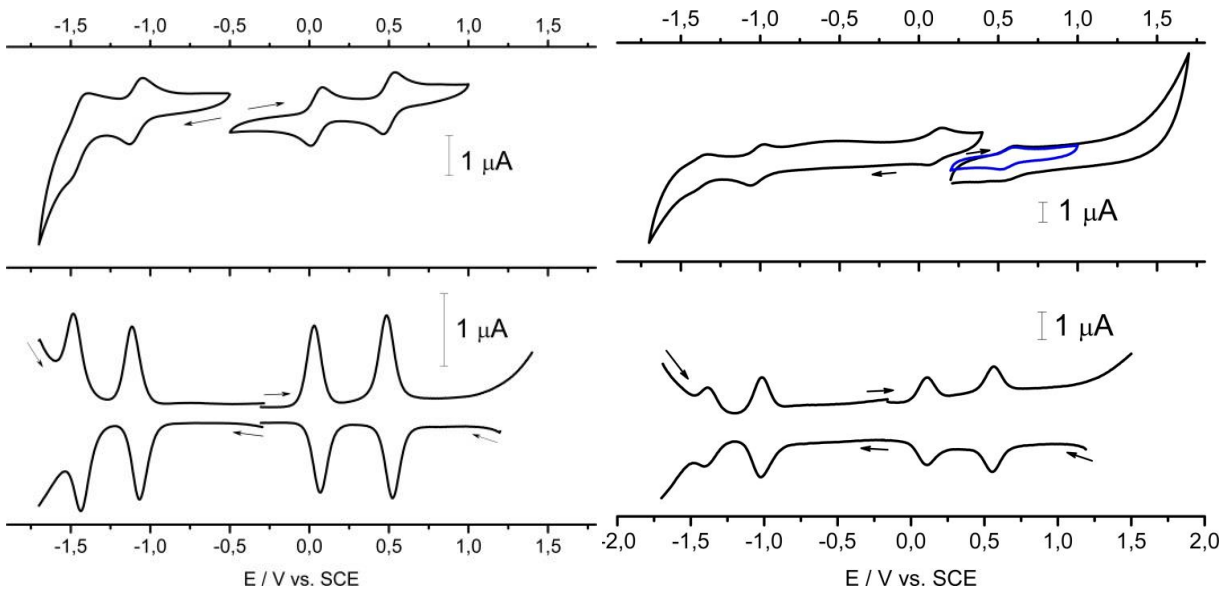

Fig. S21 CVA (scan rate 0.10 V s^{-1}) and SWVA for complexes **3b** (left) and **4b** (right) in DCB containing 0.15M $[NBu_4][BF_4]$.

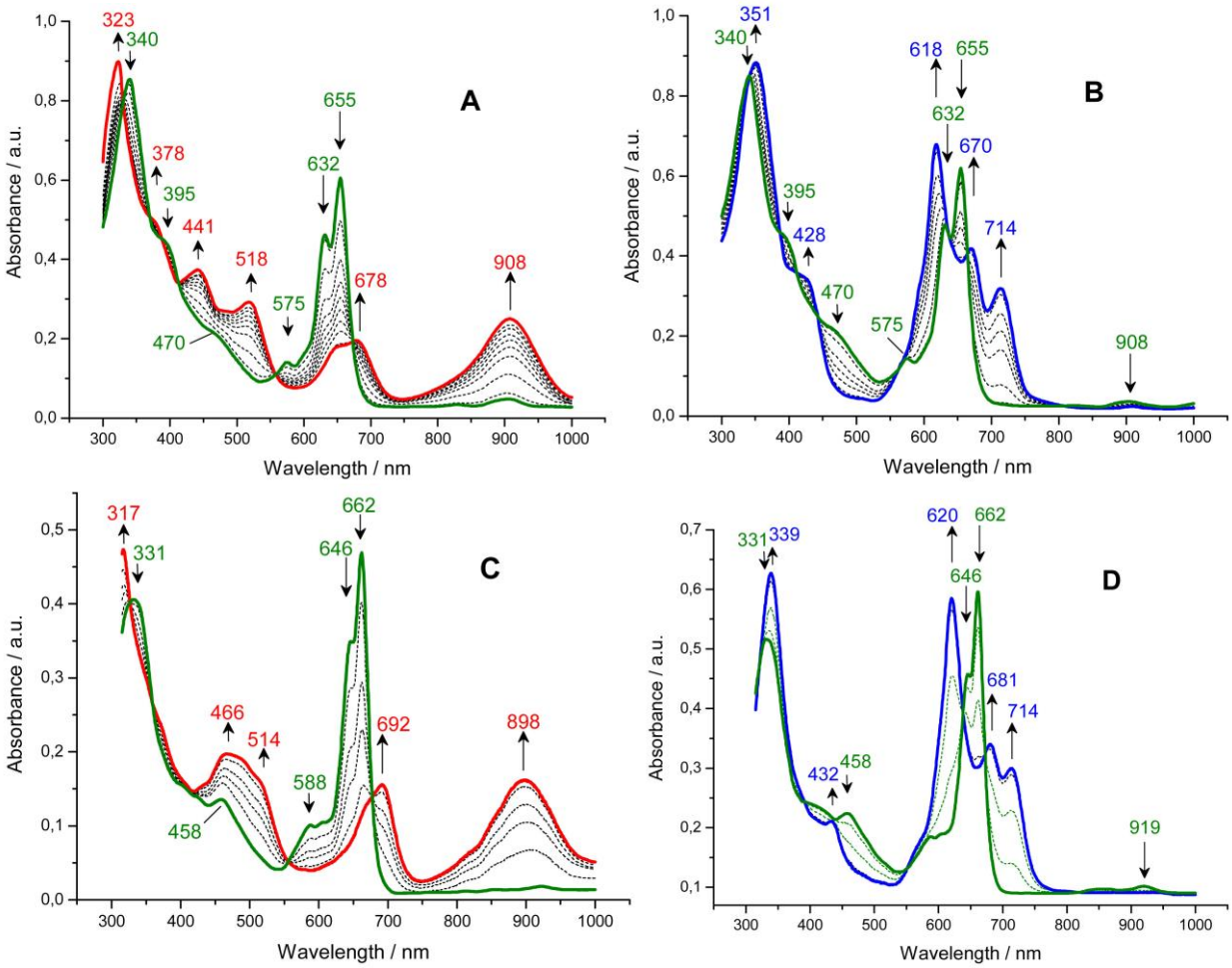

Fig. S22 UV/Vis spectral changes for **3b** and **4b** in DCB containing 0.2 M $[NBu_4][BF_4]$ during controlled-potential oxidation at +0.8 V (A, C) and reduction at –0.4 V (B, D) respectively.

Table S1 Crystallographic data and structure refinement for **3a**.

Empirical formula	$C_{78}H_{42}N_{14}Eu$
F_w	1327.23
Crystal system	Monoclinic
Space group	$P2_1/c$
a/Å	32.7080(6)
b/Å	13.4864(2)
c/Å	36.4446(7)
α (°)	90
β (°)	122.417(1)
γ (°)	90
V (Å^3)	13571.0(4)
Z	8
D_{calc} (Mg m^{-3})	1.299
μ (mm^{-1})	7.042
F (000)	5368
Crystal size (mm^3)	0.10 × 0.10 × 0.10
λ (Å)	1.54186
θ range for data collection (°)	3.59–69.25
Index ranges	$-39 \le h \le 36$; $-16 \le k \le 7$; $-44 \le l \le 35$
Reflections collected	30997
Reflections independent (R_{int})	23635 (0.0216)
Absorption correction	Empirical (DIFABS)
T_{min}/T_{max}	0.0334/0.4945
Refinement method	Full-matrix least-squares on F^2
Data/restraints/parameters	23609/1314/1627
Goodness-of-fit on F^2	0.585
R_1, wR_2 [I>2σ(I)]	0.0546, 0.0252
R_1, wR_2 (all data)	0.2168, 0.0361
$\Delta\rho_{max}$, $\Delta\rho_{min}$ (e Å^{-3})	0.547, –0.768